PHILOSOPHICAL TRANSACTIONS A

royalsocietypublishing.org/rsta

Research

Cite this article: Miyake F *et al.* 2026 Reassessment of a cosmic ray increase event in 1279/1280 CE using carbon-14 records of tree rings. *Phil. Trans. R. Soc. A* **384**: 20250264.
https://doi.org/10.1098/rsta.2025.0264

Received: 15 October 2025
Accepted: 15 December 2025

One contribution of 17 to a Theo Murphy meeting issue 'Radiocarbon and cosmic radiation events'.

Subject Areas:
solar system, astrophysics, atmospheric science

Keywords:
carbon-14, tree rings, 14C spike, solar energetic particle event, galactic cosmic rays, solar activity

Author for correspondence:
Fusa Miyake
e-mail: fmiyake@isee.nagoya-u.ac.jp

Reassessment of a cosmic ray increase event in 1279/1280 CE using carbon-14 records of tree rings

Fusa Miyake[1], A. J. Timothy Jull[2,4], Katsuhiko Kimura[5], Mihaly Molnar[4], Toru Moriya[6], Vladimir Myglan[7], Irina P. Panyushkina[3], Andrea Scifo[8], Mirei Takeyama[6], Fuyuki Tokanai[6], Ilya Usoskin[1] and Lukas Wacker[9]

[1]Institute for Space-Earth Environmental Research, Nagoya University, Nagoya, Aichi Prefecture, Japan
[2]Department of Geosciences and [3]Laboratory of Tree-Ring Research, University of Arizona, Tucson, AZ, USA
[4]Isotope Climatology and Environmental Research Centre, HUN-REN Institute for Nuclear Research, Debrecen, Hungary
[5]Fukushima University, Fukushima, Fukushima Prefecture, Japan
[6]Yamagata University, Yamagata, Yamagata Prefecture, Japan
[7]Siberian Federal University, Krasnoyarsk, Krasnoyarsk Krai, Russian Federation
[8]University of Groningen, Groningen, Netherlands
[9]Department of Physics, ETH Zurich, Zurich, Switzerland

FM, 0000-0001-8002-9601; AS, 0000-0002-7174-3966

Extreme solar energetic particle events (ESPEs) rarely occur on the Sun, as known from cosmogenic isotope proxies, the primary being ^{14}C measured in tree rings. Several such events have been identified in tree-ring ^{14}C data as sharp spikes. The most recent spike, around 1279 CE, has been reported in several previous studies, but the results were controversial. Here, we investigated the possible occurrence of an ESPE around 1279 CE by analysing new high-precision $\Delta^{14}C$ data from Japanese cedar and Altai larch tree samples for the period 1274–1288. Cross-comparisons of our datasets from different accelerator mass spectrometry

Supplementary material is available online at https://doi.org/10.6084/m9.figshare.c.8571483.

THE ROYAL SOCIETY PUBLISHING

facilities demonstrated their high reproducibility. Although our independent measurements do not yield a statistically significant single-year ^{14}C spike, the result supports a small but significant $\Delta^{14}C$ enhancement around 1279–1280. The $\Delta^{14}C$ data were analysed by using two different carbon-transport models, Ticktack and SOCOL:14C-Ex, showing a robust result. We examined possible causes for the ^{14}C increase, that is, ESPE and variations in galactic cosmic rays and concluded that the two scenarios cannot be distinguished with the existing datasets. Further investigations using ice-core records and ^{14}C data from the southern hemisphere will be crucial to determine the cause of this event.

This article is part of the Theo Murphy meeting issue 'Radiocarbon and cosmic radiation events'.

1. Introduction

The primary natural pathway of carbon-14 (^{14}C) production is via atmospheric neutrons in nuclear reactions between energetic cosmic rays and nuclei of atmospheric gases. Cosmic rays are of extraterrestrial origin and have two populations with distinct origins: omnipresent galactic cosmic rays (GCRs) and sporadic solar energetic particles (SEPs). The flux of GCRs varies in the Earth's vicinity because of factors such as the solar wind, heliospheric magnetic field and geomagnetic field, which modulate their intensity and spectrum (e.g. [1]). Sporadic solar eruptions can occasionally lead to SEP events with a greatly enhanced flux of lower-energy cosmic rays, lasting for hours to days [2]. The change in the amount of ^{14}C measured in tree rings reflects the cosmic ray flux and, thus, solar activity, including extreme SEP events (ESPEs), during the period of the tree growth. Along with ^{14}C in tree rings, other cosmogenic nuclides (e.g. ^{10}Be and ^{36}Cl in ice cores), which are also produced by cosmic rays, can be used to investigate past solar activities and enable parametric reconstruction of ESPE energy spectra (e.g. [3,4]). Notably, ^{14}C data from annual tree rings are used to identify ^{14}C spikes, which are considered signatures of ESPEs (e.g. [5,6]), and to investigate the 11-year solar Schwabe cycle (e.g. [7,8]), which are visible as small gradual ^{14}C fluctuations over 11 years.

To date, searches for ^{14}C spikes have been actively pursued with several spikes resulting from ESPEs reported for 774 CE, 993 CE, 664 BCE, 7176 BCE and 12 350 BCE (e.g. [9–13]). These ^{14}C spikes are characterized by a significant increase in ^{14}C concentrations against their measurement errors within 1–2 years, followed by a decrease in ^{14}C concentration with a time constant of about 10 years. This can be explained by a sudden influx of cosmic rays into the Earth's atmosphere, followed by a redistribution of ^{14}C between different terrestrial reservoirs owing to atmospheric circulation. Similar production spikes have also been detected in ^{10}Be and ^{36}Cl records in ice cores from Antarctica and Greenland (e.g. [3,14–17]). A multi-nuclide analysis has indicated that their origin is consistent with SEPs, and they are considered to have been caused by ESPEs with intensities exceeding those of the largest SEP event observed in the modern era by orders of magnitude [18].

There is a significant scale gap between the events detected through cosmogenic nuclides and those observed in the modern instrumental era [19]. Since intermediate-scale ESPEs have not been found, the question of the nature of the extreme events remains open—do they correspond to the far tail of the normal SEP event distribution, or form a special, presently unknown class of events? Therefore, detecting such events is a crucial challenge for understanding the characteristics of SEP events ranging from small to extreme scales. Comprehensive identification of intermediate events can clarify whether extreme SEP events and smaller events detected in modern observations share common underlying physical mechanisms. Although intermediate events are less intense than extreme ones, they still constitute solar activity unprecedented for recent decades, with potentially severe implications for the modern, highly technological society. Therefore, understanding their occurrence probabilities and characteristics is crucial for assessing the risks they may pose to modern technological society.

In addition to the major ^{14}C spikes mentioned above, several smaller-scale ^{14}C increases have been reported around 1279 CE, 1052 CE (1054 CE), 1528 BCE and 5410 BCE [7,20–22]. These ^{14}C enhancement events may be attributed to ESPEs slightly smaller than the largest events mentioned above. However, given their small ^{14}C enhancements, careful consideration is required to distinguish them from the background fluctuations of annual ^{14}C levels and to determine their origin. Additionally, these ^{14}C spikes have not yet been confirmed by ^{10}Be and ^{36}Cl data from ice cores, leaving their cause unidentified.

In particular, the ^{14}C spikes *ca* 1279 were investigated in detail in several previous studies. Originally, Brehm *et al.* [7] identified it as a significant annual increase in $\Delta^{14}C$ in their high-resolution ^{14}C dataset covering the past 1000 years. They reported a $\Delta^{14}C$ increase of 5.0‰ ± 3.2‰ occurring from 1279 to 1280 (using oak tree rings from the United Kingdom). Additionally, Miyahara *et al.* [23] reported a $\Delta^{14}C$ increase of 3.2‰ ± 0.6‰ from 1279 to 1280 based on their ultra-high-precision data of asunaro wood samples (*Thujopsis dolabrata*) from northern Japan. Meanwhile, Scifo *et al.* [24] conducted high-resolution ^{14}C analysis of another oak wood sample from the United Kingdom but failed to detect a significant ^{14}C increase (1.7‰ ± 2.3‰ from 1279 to 1280). In addition, before the 1279 event was reported, annually resolved ^{14}C data—though limited in precision and temporal resolution—had already been published, and no increase in ^{14}C concentrations was reported (e.g. [25,26]). Although these datasets exhibit an increasing trend, they show different conclusions regarding the presence or absence of the ESPE during that period. This highlights the difficulty of detecting small variations in ^{14}C concentrations and indicates that various factors—many of which are still not well understood—may influence the measured ^{14}C concentrations, such as regional or species-related differences in the trees analysed, interlaboratory variations, or systematic differences between accelerator mass spectrometry (AMS) measurements.

Here, we performed high-precision ^{14}C analyses of tree-ring samples of Japanese cedar from Yakushima Island (southern Japan) and Altai larch from Inner Eurasia (southern Russia) to clarify the presence of a statistically significance ^{14}C spike and its possible origin. We evaluated potential factors that could affect small variations in ^{14}C concentrations from the tested tree rings measured under different conditions and at different AMS facilities. Specifically, for the Japanese cedar sample, we examined (i) differences in the timing of chemical pretreatment of tree-ring samples, (ii) differences between AMS laboratories (Yamagata University [YU-AMS] and ETH Zürich), and (iii) intra-ring differences (earlywood and latewood). Finally, we analysed the obtained data, combined with previously published ones, to assess the most probable source of the spike around 1279 CE, and its characteristics.

2. Material and methods

(a) Japanese cedar

We used Japanese cedar (*Cryptomeria japonica*) from Yakushima Island, Japan (supplementary material, figure S1), which was cut in 1990. Two pieces of wood were cut from the same tree specimen and used for the analysis (Yaku-Cb and Yaku-Cc). The ages of the tree-ring samples were determined through cross-dating. The *t*-values of the two samples (Yaku-Cb and Yaku-Cc), relative to the master chronology, were $t = 6.11$ and $t = 5.38$, respectively.

The tree ring samples for the ^{14}C measurement at YU-AMS were cut with annual resolution for the period from 1275 to 1288, whereas those for the ^{14}C measurement at ETH Zürich were mainly cut into earlywood and latewood for the period from 1277 to 1284. Holo-cellulose samples were obtained from cut tree rings using the following pretreatment procedures: (1) 3 M HCl at 70°C overnight, (2) 1.2 M NaOH at 70°C overnight, (3) 3 M HCl at 70°C for 3 h, (4) bleach with a $NaClO_2$/HCl solution overnight, (5) neutralization by replacing Milli-Q water several times until the solution becomes neutral, and (6) drying the samples in an oven. Between steps 1 and 2 and between steps 2 and 3, the solution was replaced once with Milli-Q water. The chemical pretreatments for measurements at YU-AMS were conducted both in 2016 and 2021. The cutting of tree samples and chemical treatment were conducted at Nagoya University.

The graphitization processes were conducted at YU-AMS and ETH Zürich. The ^{14}C measurements at YU-AMS were performed using the compact AMS system of the National Electrostatics Corporation [27], whereas those at ETH Zürich were conducted using the MICADAS system of Ionplus [28,29]. The cellulose samples were measured one to eight times at YU-AMS and once at ETH Zürich. The years 1284, 1280 and 1278 CE of the annual ring series were measured using the same cellulose samples as those measured at YU-AMS. The averaged errors of each $\Delta^{14}C$ data are 2.2‰ and 1.9‰ for YU-AMS and ETH Zürich, respectively. A summary of the pretreatments and AMS measurements is provided in the supplementary material, tables S1 and S2.

(b) Altai Larch

Specimen 09ak36me of *Larix sibirica* was collected in 2009 from a dead snag at an elevation of 2315 m asl in the Severo-Chuyskiy Range of the Altai Mountains, near the state border between Russia and Mongolia. A photo of the Ak-Kha Forest (coordinates: 49°23.348′N, 87°25.694′E) in the Kosh-Agach District where the snag was found, is provided in the supplementary material. The tree rings of this specimen were cross-dated with the Mangun Taiga master tree-ring chronology for the period 1164–1590 CE, 0.64 inter-series correlation [30]. For annual ^{14}C analysis, 13 individual tree rings spanning 1274–1286 CE were separated at the Laboratory of Tree-Ring Research, University of Arizona.

Cellulose extraction and ^{14}C measurements were conducted at the Isotope Climatology and Environmental Research Centre (formerly the Hertelendi Laboratory of Environmental Studies) at the Institute for Nuclear Research in Debrecen, Hungary. This AMS facility uses the BABAB method to pretreat the cellulose and the sealed-tube graphitization process as described above [31]. The larch tree ring ^{14}C content was measured on the Environ-MICADAS, Ionplus system [29,32], with the measurement time and conditions pre-set on at least 200 000 net counts for every single target. Measurement uncertainty ranges from 1.87 to 2.23‰, accounting for normalization, background subtraction and counting statistics. The procedures for holo-cellulose pretreatment, graphitization and AMS measurement at the Debrecen facility are comparable to those used at ETH Zürich, with the primary difference being that samples were measured only twice. The AMS results are presented in table S2.

3. Results

The measured $\Delta^{14}C$ data of YU-AMS are shown in figure S3 and provided in the supplementary material (table S2). Each cellulose sample was measured between one and eight times. The results from repeated measurements of the same sample were consistent, with no values rejected at the 95% confidence level. Figure 1 compares ^{14}C results from identical samples that underwent chemical pretreatment in different years (2016 and 2021), with the results averaged for each sample, with no significant differences observed owing to the timing of chemical pretreatment.

Figure 2 shows the results from ETH Zürich. The average difference between latewood and earlywood was 1.3‰ ± 0.9‰ (L − E), which is not a statistically significant difference with the given measurement uncertainty. We also measured the annual rings for the years 1284, 1280 and 1278 CE, using the same cellulose samples prepared for the YU-AMS analysis. The results of these annual rings for 3 years were consistent with those of the earlywood and latewood. Therefore, the cedar measurements from each AMS facility were averaged for each calendar year. Figure 3 compares the two AMS facilities, showing consistent results within the margin of error for $\Delta^{14}C$, despite the small uncertainties of approximately 1‰.

Meanwhile, the result for the Altai larch showed a significant offset with the Japanese cedar series, as shown in figure 4. The Altai larch series showed a 4.3‰ ± 0.7‰ higher $\Delta^{14}C$ value compared with the Japanese cedar on average. Excluding this offset, the two datasets showed similar trends in ^{14}C variations, and the significant increase from 1279 to 1280 CE reported in previous

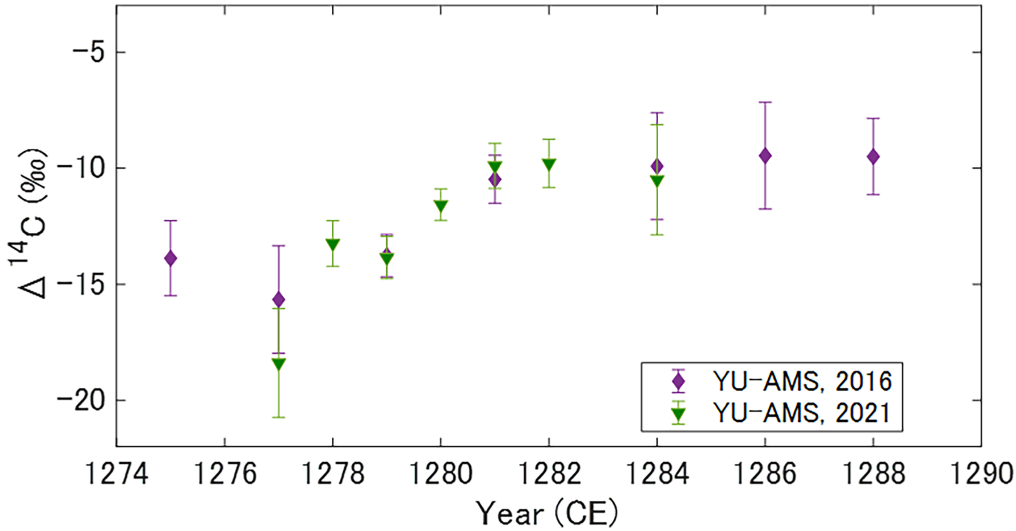

Figure 1. Measured $\Delta^{14}C$ dataset at YU-AMS. Diamonds and triangles represent data from cellulose samples pretreated in 2016 and 2021, respectively. Each data point is the average of one to eight measurements.

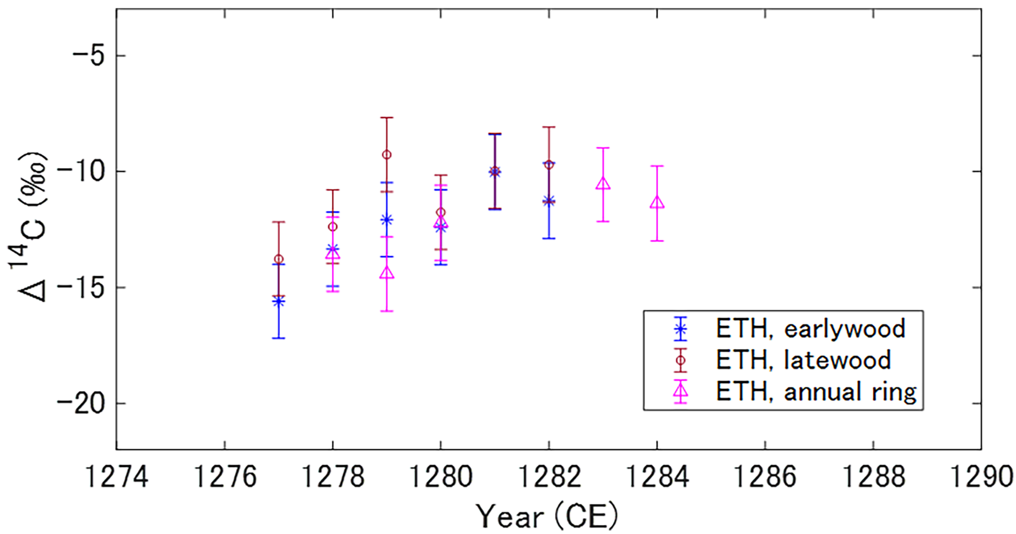

Figure 2. Measured $\Delta^{14}C$ datasets at ETH Zürich. Stars, circles and triangles indicate earlywoods, latewoods and annual rings, respectively.

studies was not observed in either series—1.4‰ ± 0.8‰ (Japanese cedar) and 3.1‰ ± 2.8‰ (Altai larch) from 1279 to 1280 CE. However, over a 2-year period from 1279 to 1281 CE, larger increases were observed in both series, i.e. 3.1‰ ± 0.8‰ (Japanese cedar) and 4.2‰ ± 2.7‰ (Altai larch).

4. Discussion

(a) Comparison between datasets

The current datasets were compared with high-precision annual ^{14}C datasets of previous studies [7,23–25], as illustrated in figure 5. All series show an increasing trend around 1280 CE; a significant

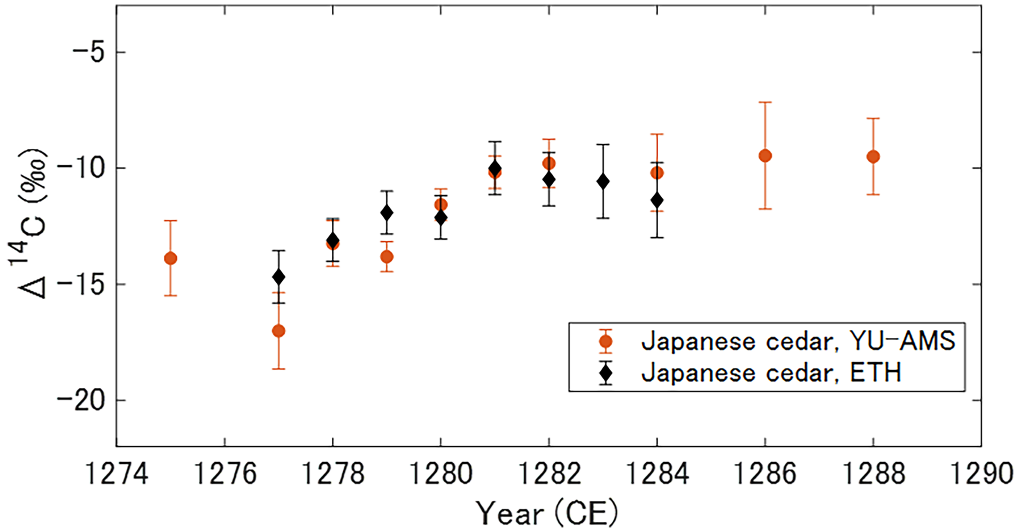

Figure 3. Comparison of the annual averages of $\Delta^{14}C$ values of Japanese cedar measured at Yu-Ams and ETH Zürich.

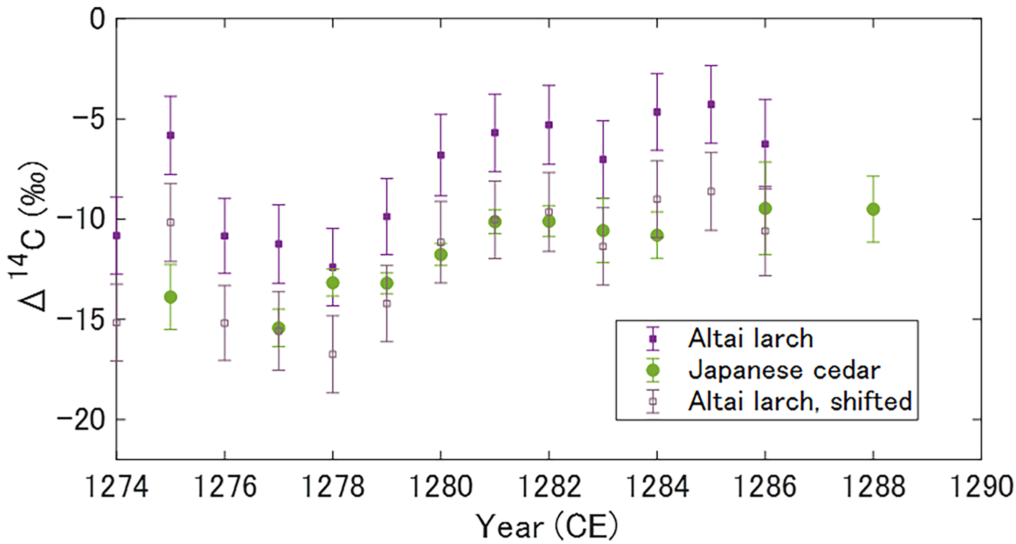

Figure 4. Comparison between Japanese cedar (circles) and Altai larch (squares). Open squares represent the dataset after offset correction (i.e. shifted by 4.3‰).

offset exists between several datasets. Table 1 lists the weighted-average offsets of different data series relative to the dataset based on Japanese cedar. Only Scifo *et al.* [24] showed good agreement with no significant offset comparing the Japanese cedar and the UK oak, whereas the other series exhibited significant offsets of 3‰–5‰.

Previous studies suggested a latitudinal gradient in tree-ring ^{14}C records, so that data from higher latitude regions tend to have higher ^{14}C values than from tropical regions. This is seen as observed offsets of approximately 3‰ and 1‰ between NH0 (high latitude; greater than 60° north latitude) zone on the one hand, and NH2 (mid-latitude; less than 45° north latitude) and NH1 (latitude 45–60°) zone on the other hand, respectively [33,34]. Yakushima Island, where the Japanese cedar was growing, is in the NH2 radiocarbon zone, whereas most of the other tree

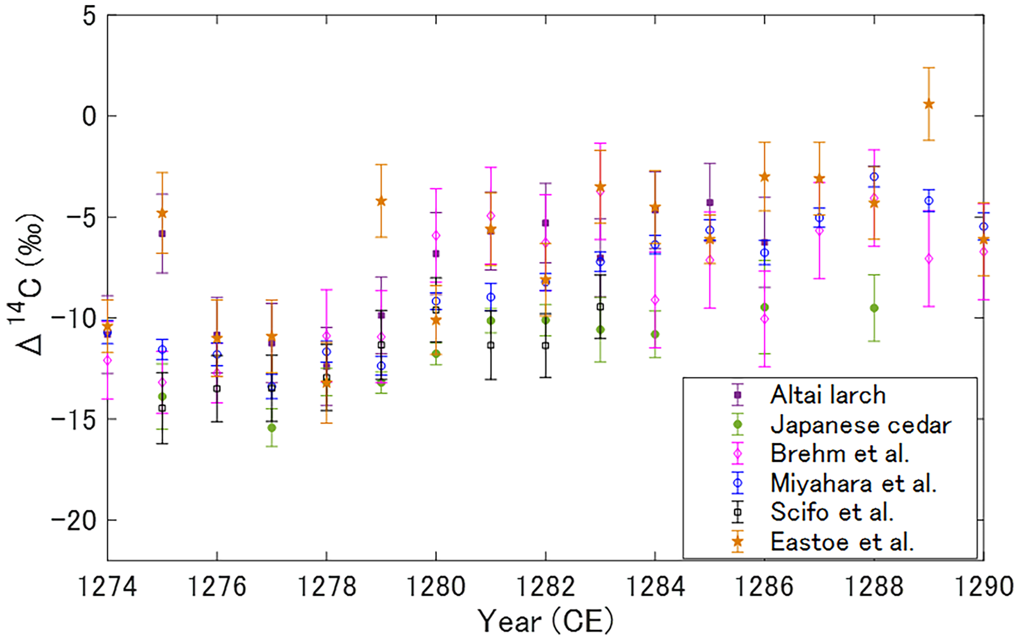

Figure 5. Comparison with previous studies, i.e. Irish oak [7,24], Japanese asunaro [23] and US sequoia [25].

Table 1. Summary of differences between Japanese cedar on the one hand, and Altai larch (this study), UK oak [7], Japanese asunaro [23], and UK oak [24] series, on the other hand.

	Altai larch (this study)	UK oak (Brehm *et al.* [7])	Japanese asunaro (Miyahara *et al.* [23])	UK oak (Scifo *et al.* [24])	US sequoia (Eastoe *et al.* [25])
weighted-average offset versus Japanese cedar	4.3‰ ± 0.7‰	3.3‰ ± 0.8‰	2.1‰ ± 0.3‰	0.6‰ ± 0.7‰	4.8‰ ± 0.6‰
total χ^2 value without offset correction (dof)	42.9 (10)	24.4 (10)	62.6 (11)	5.1 (8)	75.0 (11)
total χ^2 value after offset correction (dof)	6.5 (10)	7.3 (10)	16.2 (11)	4.4 (8)	19.9 (11)
radiocarbon zone	NH1	NH1	NH1	NH1	NH2

Note: The total χ^2 value is calculated as: $\sum_{t=1}^{dof} \frac{(\Delta^{14}C_{cedar,t} - \Delta^{14}C_{each\ series,t})^2}{(error_{cedar,t}{}^2 + error_{each\ series,t}{}^2)}$. The uncertainty of the offset itself was not propagated in the offset correction. The radiocarbon zone of the Japanese cedar is NH2.

sample sites in figure 5 are located in the NH1 zone. Therefore, the observed ^{14}C offsets support previously observed latitudinal differences. However, the magnitudes of the observed offsets were not uniform across datasets, and the offset observed between the UK oak samples (2.9‰ ± 0.9‰, Brehm *et al.* 2021 series [7] minus Scifo *et al.* 2024 series [24]) could not be explained by latitudinal differences alone. Furthermore, despite differences in radiocarbon zones, a significant offset was observed among tree samples from different regions within Japan. This implies that the offsets were not solely owing to latitude; instead, other geographical or environmental factors might have contributed as well.

For example, there is a notable difference in the length of the growing season among the tree species used in this study. Japanese cedar (*Cryptomeria japonica*) and English oak (*Quercus robur*) both exhibit relatively long growing seasons, typically lasting approximately 6.5 to 7 months—from April through October. By contrast, *Larix sibirica* growing at the upper tree line in the Altai Mountains (2315 m asl) forms annual rings over a much shorter period of approximately 3.5 months, from mid-May to early September. This substantial difference in growing season length reflects a key variation in the seasonal window, during which these trees assimilate carbon and exchange gases with atmospheric CO_2. In particular, the larch at high elevation operates under a short photosynthetic period driven by colder and drier climatic conditions of the inner continent, while the cedar and oak benefit from a longer period and mild weather in the marine lowland environment. These divergent carbon uptake and temporal windows can be important considerations when comparing radiocarbon signals across species and regions. Further research, including full spatially resolved carbon transport modelling, is needed to clarify their underlying causes.

Although the cause of the offsets remains unclear, a simple ad hoc shift of the data series by the average offset values (table 1) makes most datasets consistent with that of the Japanese cedar series, as indicated by the low total χ^2 values. The difference between the Japanese cedar and the Japanese asunaro series, as well as between the Japanese cedar and the US sequoia series, remained relatively large, as indicated by the total χ^2 values. This discrepancy can be attributed to factors such as differences in measurement methods (note that the US sequoia was measured by liquid scintillation counting rather than AMS), underestimation of uncertainties, or regional characteristics. As suggested by Nakamura *et al.* [35], atmospheric ^{14}C concentrations in Japan may be influenced by the southward transport of low-^{14}C-concentration air masses during certain periods, and such effects may be reflected in the observed data.

After the correction for the offsets, different datasets were found to be consistent with each other. Whereas the increase over a single year is not significant relative to the measurement uncertainty, a significant increase of 3.1‰ ± 0.8‰ (for the Japanese cedar) is observed over 2 years from 1279 to 1281 CE. This implies that increased ^{14}C production owing to enhanced cosmic ray flux occurred during that period. Below, we consider two possible causes for this ^{14}C increase: an ESPE and a significant variation in the GCR flux in the course of a solar cycle.

(b) Origin of ^{14}C increase: an ESPE

Here, we analysed the time profiles of the measured Δ^{14}C datasets for the signature of a possible ESPE. This was done by fitting the modelled Δ^{14}C curve for an ESPE to the measured data. We used different models and fitting methods to control the result's robustness.

First, we estimated the ^{14}C production rate from the Japanese cedar ^{14}C series using the Ticktack package based on a carbon-cycle box model [24,36]. In this package, the carbon cycle is modelled with the 22-box model [7], and the spike-only method was applied (details are provided in [24,36]). The fitting of the Δ^{14}C dataset was done by the Markov Chain Monte Carlo (MCMC) method, allowing us to assess the probability density function, and the most probable parameter values and their uncertainties (see details in Zhang *et al.* [36]). The fitted Δ^{14}C profiles and the corresponding ^{14}C production rates are shown in the supplementary material, figure S4. From the output of the Ticktack analysis, provided in figure 6, we obtained that the most probable ^{14}C production rate increase for the event was $1.37^{+0.28}_{-0.15}$ (atoms cm^{-2} s^{-1}), while the parameters for the Start Date and Duration were unconstrained, and a range of values fit the data, a precise determination was not achievable. The production rate is given assuming the event distribution of production over the Earth's surface during 1 year. This corresponds to $(2.21^{+0.45}_{-0.24})\times10^{26}$ atoms of ^{14}C produced globally during the event. As seen in figure 6, the duration of the ^{14}C production episode cannot be well identified from an instant injection up to 3 years. However, the central date of the production episode is robustly defined as late 1279 to early 1280 CE (see the supplementary material, figure S4).

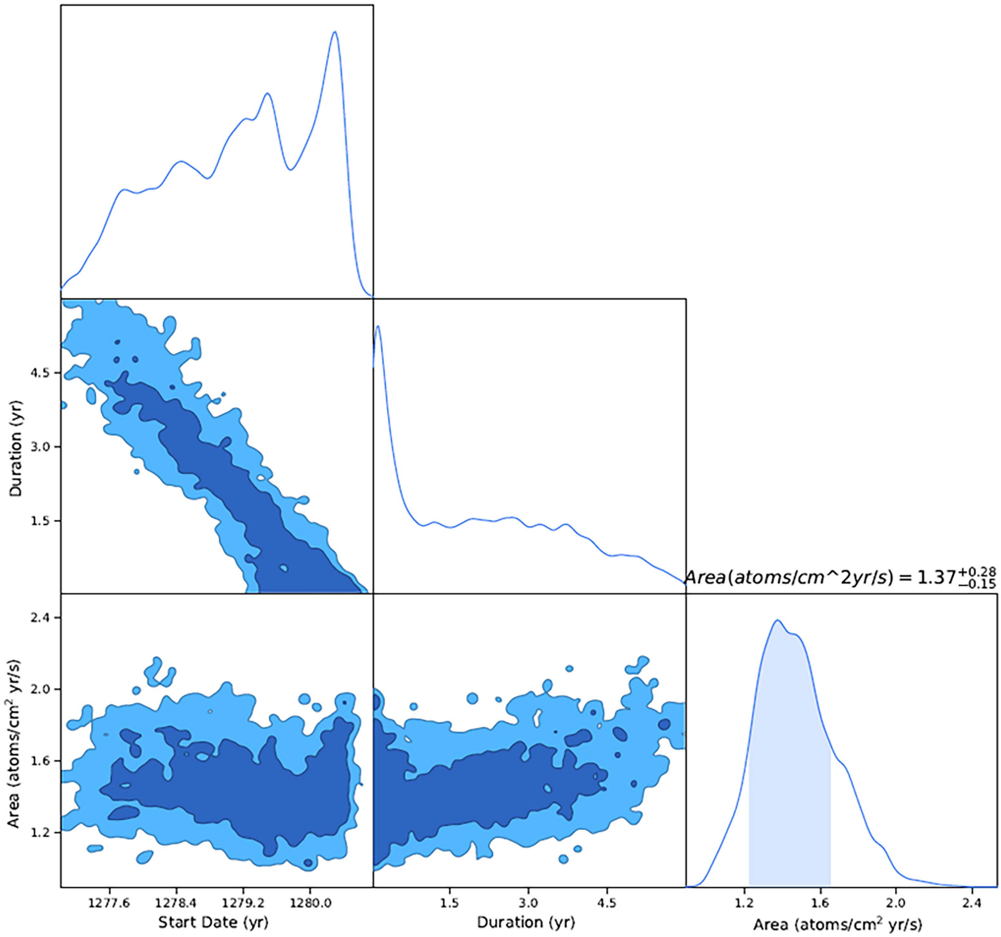

Figure 6. Output of the Ticktack analysis (start date, duration and area of ^{14}C production) on the Japanese cedar ^{14}C series. The unit of 'area' represents the ^{14}C production rate, assuming that the production occurred over a 1-year period. The plots on the diagonal represent the marginal probability distributions. Dark blue and light blue areas represent 68.2% and 95.4% highest posterior density intervals, respectively.

Next, we independently applied a similar analysis to all six time series available for this period (Japanese cedar, Russian larch, four series of previous studies). The modelled $\Delta^{14}C$ time profiles were computed by the full three-dimensional dynamic model of carbon atmospheric transport SOCOL:14C-Ex [37] for a daily ^{14}C production spike. The SOCOL model considers a realistic three-dimensional spatial distribution of the ^{14}C production in both lateral and altitude directions. The production was computed within the SOCOL framework by using the CRAC:14C production model for a realistic geomagnetic field parameterization and applying the SEP energy spectrum for a reference ESPE [37]. The data were corrected for the offset using values from table 1. Fitting of the data for the period 1278–1285 CE (51 data points) was performed by two methods: a standard one based on χ^2 statistics [37], and an MCMC one with the RMSE as the merit function (supplementary material). The results are shown in the supplementary material, figure S5. As seen, both methods yield very consistent parameter ranges: the best-fit estimate of the event occurrence date was at the turn of 1279/1280 CE, but uncertainties are as large as a half-year around it; the total ^{14}C production was $(2.6 \pm 0.6) \times 10^{26}$ atoms, or 1.6 ± 0.3 atoms cm^{-2} s^{-1} for the global average annual production rate.

Table 2. Summary of the fitting of data for the ^{14}C increase. The columns represent: the fitted datasets; the used model of carbon transport; fitting method; the estimated total amount Q of ^{14}C produced by the event; central date and duration of the production episode; and the figure where the fitting details are shown. The last line provides a summary of the three estimates, the value of Q is the weighted average of the individual Q values in the three lines above it.

dataset	model	method	Q (10^{26} atoms)	central date	duration	see figure
Japanese cedar	Ticktack	MCMC	$2.21^{+0.45}_{-0.24}$	early 1280	0–4 years	6 and S4
all data	SOCOL	MCMC	2.6 ± 0.4	Jan 1280	0–1 years	S5b, S5c
all data	SOCOL	χ^2	2.7 ± 0.7	Mar 1280	0–1 years	S5a
summary	–	–	2.4 ± 0.3	early 1280	0–3 years	

The results of the fittings are summarized in table 2. As seen, all the methods yield similar results, viz. the additional production of radiocarbon was approximately 2.4×10^{26} atoms (equivalent of the globally averaged annual production rate of 1.5 ± 0.2 atoms/cm^2/s). This value generally agrees with those of previous studies: 2.5 ± 0.6 [7], 1.5 ± 0.3 [23] and $1.10^{+0.36}_{-0.32}$ atoms/cm^2/s [24]. We note that the previous estimates were based on smaller statistics, while we used all available datasets here. For comparison, the background ^{14}C production rate owing to GCR was estimated as 1.8 atoms/cm^2/s (averaged over the period from 1265 to 1275 [7]). The fitting procedures assume the constant GCR-based Δ^{14}C background throughout the event, which may not be true for this event. Because of the probably steadily increasing ^{14}C trend (see below), the production rate might be somewhat overestimated.

The central date of the production episode is constrained to the winter 1279/1280 CE, but its duration is not well constrained. The most probably production episode is a very short/instant ^{14}C injection (see figure 6), corresponding to an ESPE scenario. In this framework, ^{14}C was dominantly produced in the Northern polar stratosphere, where it was locked by the polar vortex until the vortex's break in Spring. After that, ^{14}C was transported within the stratosphere and then flushed to the troposphere during the stratosphere-troposphere exchange, which also takes place in Boreal Spring. Because transport in the stratosphere is slow, not all radiocarbon appeared in the troposphere during the first year (1280 CE), and it took additional time to fully descend to the troposphere. This may explain the fact that Δ^{14}C rose during two consecutive years. However, a longer production episode, up to 3–4 years, centred at 1280 CE, cannot be excluded (see figure 6) and is also a valid scenario. Such a scenario may imply enhanced GCR production owing to a weak solar cycle.

(c) Origin of ^{14}C increase: GCR modulation

We also examined whether the ^{14}C increase *ca* 1280 CE could be explained by an enhanced GCR flux during a weak solar cycle minimum. On one hand, typical Δ^{14}C variations associated with the Schwabe cycle are approximately 1‰, up to approximately 2‰ (e.g. [7]). On the other hand, during the periods of grand solar minima, such as the Maunder Minimum in 1615–1700 CE, an extended Δ^{14}C increase was observed at an average rate of approximately 0.24‰ per year, with a maximum of approximately 0.5‰ per year in the IntCal20 dataset [38]. The period studied here was around the beginning of the Wolf grand solar minimum of solar activity in 1270–1340 CE [39], characterized by a systematic rise of ^{14}C production.

To disentangle the effects on different timescales, we applied the non-parametric empirical mode decomposition (EMD) analysis [40] to the Δ^{14}C data. The result is shown in figure 7. As seen, the Δ^{14}C signal can be decomposed into two empirical modes: EM1, representing a general trend of approximately 0.5‰ yr^{-1}; and EM2 as a nearly sinusoidal wave with approximately a 9-year period and 1‰ amplitude. The sum of these two modes describes the data well—the total

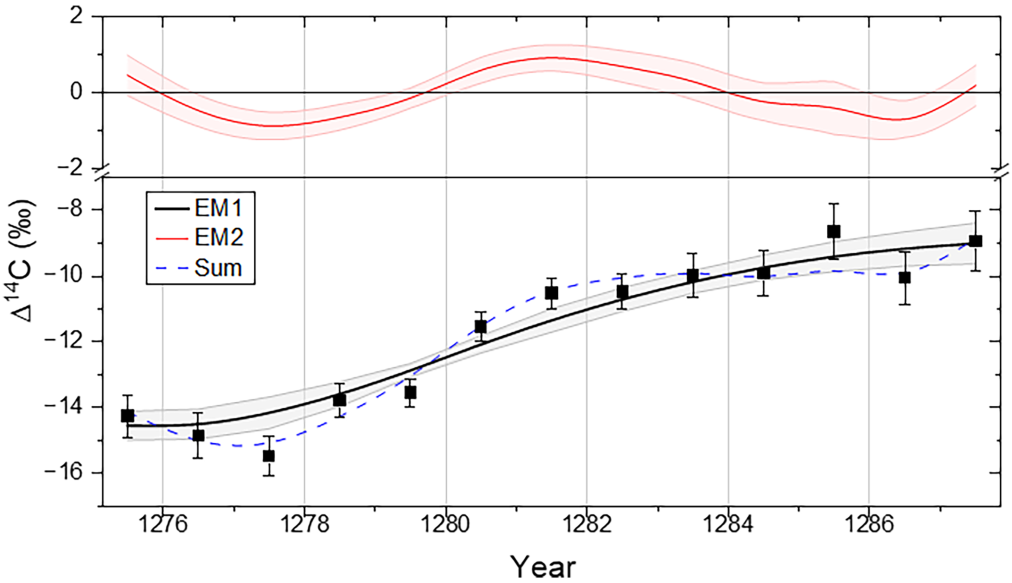

Figure 7. Empirical mode decomposition of the analysed $\Delta^{14}C$ time series: primary mode EM1 (black curve), and the secondary mode EM2 (red), along with their 68% confidence intervals, defined by MCMC. The dashed blue line depicts their sum. The black dots denote the annual $\Delta^{14}C$ data weighted-averaged over the five series (Japanese cedar, Russian larch, two US oaks and Japanese asunaro) analysed here.

value of χ^2 is 4.7 for 13 ^{14}C data points. This suggests that a combination of the increasing trend at the beginning of the Wolf grand minimum on the one hand and an 11-year solar cycle on the other hand can potentially produce the observed enhancement. To illustrate this GCR scenario, in the supplementary material, figure S6 shows a fitting result of the Japanese cedar data using four models: Schwabe cycles (sine wave) with amplitudes of 1‰ and 2‰ and combinations of the Schwabe cycle (with amplitudes of 1‰ and 2‰) and a linear trend of 0.5‰ yr^{-1}. Only the model with a Schwabe cycle with an amplitude of 1‰ showed a relatively poor fit and was rejected at the 5% significance level. A full modelling of the ^{14}C production and transport for such a scenario is planned for a forthcoming work. Furthermore, if the 0.5‰ yr^{-1} trend owing to the Grand Solar Minimum exists in $\Delta^{14}C$ data, the intensity of the ESPE discussed in the previous section would be reduced by approximately 30–40%.

Radiocarbon data from the southern hemisphere would allow us to constrain it better. Because of the different seasonal patterns in the two hemispheres, the time profile of $\Delta^{14}C$ in the southern hemisphere would be different, during the first couple of years, from that in the northern hemisphere for the ESPE scenario, but very similar for the GCR scenario. Moreover, high-resolution data of ^{10}Be and ^{36}Cl from polar ice cores can be useful to distinguish between the sources of cosmic rays causing the event (e.g. [3,41]).

5. Conclusions

We presented new high-precision measurements of $\Delta^{14}C$ in Japanese cedar and Altai larch tree ring samples for the period 1275–1288 CE to study, in detail, a small ^{14}C increase *ca* 1280 CE reported earlier. To verify the reproducibility of the Japanese cedar ^{14}C measurements, we examined potential variations owing to earlywood and latewood, differences in the timing of chemical pretreatment and measurements conducted at two independent AMS facilities (YU-AMS and ETH Zürich). These verifications yielded highly reproducible results. The new ^{14}C records from the Japanese cedar and Altai larch samples did not confirm the previously reported single-year ^{14}C

spike from 1279 to 1280 CE, but they showed a noticeable increase in ^{14}C concentrations extended over 2 years.

A significant systematic offset of 4.3‰ ± 0.7‰ was observed between the Japanese cedar and Altai larch series. We also compared our results with other available datasets. The Japanese cedar series showed good agreement with the UK oak series of Scifo *et al.* [24] with no offset, but showed offsets compared with different UK oak series, as well as another dataset from a Japanese tree. These discrepancies could not be explained solely by latitudinal differences, suggesting the influence of additional geographic or methodological factors. The offsets may also have varied over time. Most of the differences among the data series can be resolved by simply vertically shifting the datasets using their average offsets, indicating that the variations beyond the offsets are well reproduced. Further research is needed to clarify the causes of these offsets.

To investigate the cause of the observed ^{14}C increase, we modelled the ^{14}C concentration variations for two scenarios: an ESPE and an unusual GCR modulation. For the ESPE scenario, redundant modelling was performed by applying two carbon transport models, viz. the box model Ticktack and the full three-dimensional dynamical model SOCOL:14C-Ex, and two data fitting methods, viz. MCMC and χ^2. The results showed that the observed ^{14}C data could be explained by a moderate ESPE ($(2.4 \pm 0.3) \times 10^{26}$ produced ^{14}C atoms, corresponding to the global annual production rate 1.44 ± 0.16 atoms cm^{-2} s^{-1}), which occurred in the very beginning of the year 1280 CE. For the GCR scenario, we performed an EMD analysis of the available $\Delta^{14}C$ datasets and found that the data can also be well explained by a combination of a linear trend (approx. 0.5‰ yr^{-1}), probably caused by the onset of the Wolf Grand Minimum, and a nearly sinusoidal component suggesting a Schwabe cycle, with the amplitude and period that best explain the data being approximately 1‰ and 9 years, respectively. Full modelling of the GCR scenario is still pending. For future studies aiming to detect smaller SEP events, theoretical investigations into the upper limits of cosmogenic isotope production caused by GCRs will be essential.

Thus, with the existing data, we cannot distinguish between the two scenarios and confirm or reject the ESPE origin of the studied increase. While previous studies identified events by detecting statistically significant single-year increases in ^{14}C concentrations, our study highlights that variations in GCRs could provide a plausible alternative explanation, particularly for smaller events. Potentially, high precision ^{14}C data from the southern hemisphere, as well as the annually resolved measurements of other cosmogenic isotopes ^{10}Be and ^{36}Cl in ice cores, could allow us to resolve the ambiguity and specify the origin of the 1279/1280 CE event.

Data accessibility. 14C data are provided in the supplementary information [42].

Declaration of AI use. AI was used to check English grammar.

Authors' contributions. F.M.: conceptualization, data curation, formal analysis, funding acquisition, investigation, methodology, project administration, resources, visualization, writing—original draft, writing—review and editing; A.J.T.J.: data curation, funding acquisition, investigation; K.K.: data curation, investigation, resources, writing—review and editing; M.M.: data curation, investigation, resources; T.M.: data curation, investigation; V.M.: data curation, investigation, resources; I.P.P.: conceptualization, data curation, funding acquisition, investigation, resources, writing—original draft, writing—review and editing; A.S.: data curation, formal analysis, investigation, methodology, writing—original draft, writing—review and editing; M.T.: data curation, investigation; F.T.: data curation, investigation, resources; I.U.: conceptualization, data curation, formal analysis, funding acquisition, investigation, methodology, visualization, writing—original draft, writing—review and editing; L.W.: data curation, investigation, resources, writing—review and editing.

All authors gave final approval for publication and agreed to be held accountable for the work performed therein.

Conflict of interest declaration. We declare we have no competing interests.

Funding. F.M.'s work was supported by JSPS Grant-in-Aids JP20K20918, JP20H05643, JP20H00035, JP20H01369, JP23H00135 and JP25H00635, and by the RDP Program Aiming at Maximizing the Career Potential of Female Researchers, Nagoya University (MEXT's Initiative for Realizing Diversity in the Research Environment, Leadership training type for women). I.P. and A.J.T.J. were supported by NASA grant 80NSSC21K1426. I.U. acknowledges partial support from the European Research Council Synergy Grant (project 101166910).

Acknowledgements. We thank Shozo Ohta and Chihiro Mori for the sample preparations. We thank the ISSI international team activity (510; SEESUP) and the Royal Society meeting (Radiocarbon and cosmic radiation events) for fruitful discussions, which served as the starting point for this study.

References

1. Potgieter MS. 2013 Solar modulation of cosmic rays. *Living Rev. Sol. Phys.* **10**, 3. (doi:10.12942/lrsp-2013-3)
2. Desai M, Giacalone J. 2016 Large gradual solar energetic particle events. *Living Rev. Sol. Phys.* **13**, 3. (doi:10.1007/s41116-016-0002-5)
3. Mekhaldi F *et al.* 2015 Multiradionuclide evidence for the solar origin of the cosmic-ray events of AD 774/5 and 993/4. *Nat. Commun.* **6**, 1–8. (doi:10.1038/ncomms9611)
4. Koldobskiy S, Mekhaldi F, Kovaltsov G, Usoskin I. 2023 Multiproxy reconstructions of integral energy spectra for extreme solar particle events of 7176 BCE, 660 BCE, 775 CE, and 994 CE. *J. Geophys. Res. Space Phys.* **128**, e2022JA031186. (doi:10.1029/2022JA031186)
5. Usoskin IG, Kromer B, Ludlow F, Beer J, Friedrich M, Kovaltsov GA, Solanki SK, Wacker L. 2013 The AD775 cosmic event revisited: the Sun is to blame. *A&A* **552**, L3. (doi:10.1051/0004-6361/201321080)
6. F Miyake, IG Usoskin, S Poluianov (eds). 2019 *Extreme solar particle storms*, Bristol, UK: IOP Publishing. (doi:10.1088/2514-3433/ab404a)
7. Brehm N *et al.* 2021 Eleven-year solar cycles over the last millennium revealed by radiocarbon in tree rings. *Nat. Geosci.* **14**, 10–15. (doi:10.1038/s41561-020-00674-0)
8. Usoskin IG, Solanki SK, Krivova NA, Hofer B, Kovaltsov GA, Wacker L, Brehm N, Kromer B. 2021 Solar cyclic activity over the last millennium reconstructed from annual ^{14}C data. *A&A* **649**, A141. (doi:10.1051/0004-6361/202140711)
9. Miyake F, Nagaya K, Masuda K, Nakamura T. 2012 A signature of cosmic-ray increase in AD 774–775 from tree rings in Japan. *Nature* **486**, 240–242. (doi:10.1038/nature11123)
10. Miyake F, Masuda K, Nakamura T. 2013 Another rapid event in the carbon-14 content of tree rings. *Nat. Commun.* **4**, 1748. (doi:10.1038/ncomms287310.1038/ncomms2783)
11. Panyushkina IP *et al.* 2024 The timing of the ca-660 BCE Miyake solar-proton event constrained to between 664 and 663 BCE. *Commun. Earth Environ.* **5**, 454. (doi:10.1038/s43247-024-01618-x)
12. Brehm N *et al.* 2022 Tree-rings reveal two strong solar proton events in 7176 and 5259 BCE. *Nat. Commun.* **13**, 1–1198. (doi:10.1038/s41467-022-28804-9)
13. Bard E, Miramont C, Capano M, Guibal F, Marschal C, Rostek F, Tuna T, Fagault Y, Heaton TJ. 2023 A radiocarbon spike at 14 300 cal yr BP in subfossil trees provides the impulse response function of the global carbon cycle during the Late Glacial. *Phil. Trans. R. Soc. A* **381**, 20220206. (doi:10.1098/rsta.2022.0206)
14. Miyake F, Suzuki A, Masuda K, Horiuchi K, Motoyama H, Matsuzaki H, Motizuki Y, Takahashi K, Nakai Y. 2015 Cosmic ray event of A.D. 774–775 shown in quasi-annual ^{10}Be data from the antarctic Dome Fuji Ice Core. *Geophys Res. Lett.* **42**, 84–89. (doi:10.1002/2014GL062218)
15. Miyake F, Horiuchi K, Motizuki Y, Nakai Y, Takahashi K, Masuda K, Motoyama H, Matsuzaki H. 2019 ^{10}Be signature of the cosmic ray event in the 10th century CE in both hemispheres, as confirmed by quasi-annual ^{10}Be data from the Antarctic Dome Fuji ice core. *Geophys Res. Lett.* **46**, 11–18. (doi:10.1029/2018GL080475)
16. O'Hare P *et al.* 2019 Multiradionuclide evidence for an extreme solar proton event around 2,610 B.P. (∼660 BC). *Proc. Natl Acad. Sci. USA* **116**, 5961–5966. (doi:10.1073/pnas.1815725116)
17. Paleari CI *et al.* 2022 Cosmogenic radionuclides reveal an extreme solar particle storm near a solar minimum 9125 years BP. *Nat. Commun.* **13**, 214. (doi:10.1038/s41467-021-27891-4)
18. Usoskin I *et al.* 2023 Extreme Solar events: setting up a paradigm. *Space Sci. Rev.* **219**, 73. (doi:10.1007/s11214-023-01018-1)
19. Usoskin IG, Kovaltsov GA. 2021 Mind the gap: new precise ^{14}C data indicate the nature of extreme solar particle events. *Geophys. Res. Lett.* **48**, e2021GL094848. (doi:10.1029/2021GL094848)
20. Terrasi F *et al.* 2020 Can the ^{14}C anomaly in 1054 CE be due to SN1054? *Radiocarbon* **62**, 1403–1418. (doi:10.1017/RDC.2020.58)
21. Pearson C, Wacker L, Bayliss A, Brown D, Salzer M, Brewer P, Bollhalder S, Boswijk G, Hodgins G. 2020 Annual variation in atmospheric 14C between 1700 BC and 1480 BC. *Radiocarbon* **62**, 939–952. (doi:10.1017/RDC.2020.14)

22. Miyake F *et al.* 2021 A single-year cosmic ray event at 5410 BCE registered in ^{14}C of tree rings. *Geophys Res. Lett.* **48**, e2021GL093419. (doi:10.1029/2021GL093419)
23. Miyahara H, Tokanai F, Moriya T, Takeyama M, Sakurai H, Ohyama M, Horiuchi K, Hotta H. 2022 Recurrent large-scale solar proton events before the onset of the Wolf Grand solar minimum. *Geophys. Res. Lett.* **49**, e2021GL097201. (doi:10.1029/2021gl097201)
24. Scifo A, Abi Nassif T, Conti M, Bayliss A, Doeve P, Dee MW. 2024 New data fails to replicate the small-scale radiocarbon anomalies in the early second millennium CE. *Radiocarbon* **66**, 518–531. (doi:10.1017/RDC.2024.52)
25. Eastoe CJ, Tucek CS, Touchan R. 2019 Δ14C and δ13C in annual tree-ring samples from sequoiadendron giganteum, AD 998–1510: solar cycles and climate. *Radiocarbon* **61**, 661–680. (doi:10.1017/RDC.2019.27)
26. Fogtmann-Schulz A, Baittinger C, Karoff C, Olsen J, Knudsen MF. 2020 Changes in solar activity during the Wolf Minimum – new insights from a high-resolution ^{14}C record based on Danish oak. *Radiocarbon* **63**, 91–104. (doi:10.1017/RDC.2020.126)
27. Takeyama M *et al.* 2024 Present status of the YU-AMS system and its operation over the past 10 years. *Nucl. Instrum. Methods Phys. Res. B* **538**, 30–35. (doi:10.1016/j.nimb.2023.01.021)
28. Wacker L *et al.* 2010 Micadas: routine and high-precision radiocarbon dating. *Radiocarbon* **52**, 252–262. (doi:10.1017/S0033822200045288)
29. Sookdeo A *et al.* 2020 Quality dating: a well-defined protocol implemented at ETH for high-precision ^{14}C-dates tested on late glacial wood. *Radiocarbon* **62**, 891–899. (doi:10.1017/RDC.2019.132)
30. Myglan VC, Oydupaa OC, Vaganov EA. 2013 Development of 2,367-year tree-ring chronology for the Altai-Sayan region (Mongun-Taiga mountain range). *Archaeol. Ethnogr. Anthropol. Eurasia* **3**, 51. (doi:10.1016/j.aeae.2012.11.009)
31. Molnár M *et al.* 2013 Status report of the new AMS ^{14}C sample preparation lab of the Hertelendi Laboratory of Environmental Studies (Debrecen, Hungary). *Radiocarbon* **55**, 665–676. (doi:10.1017/S0033822200057829)
32. Němec N, Wacker L, Hajdas I, Gäggeler H. 2010 Alternative methods for cellulose preparation for AMS measurement. *Radiocarbon* **52**, 1358–1370. (doi:10.1017/S0033822200046440)
33. Büntgen U *et al.* 2018 Tree rings reveal globally coherent signature of cosmogenic radiocarbon events in 774 and 993 CE. *Nat. Commun.* **9**, 3605. (doi:10.1038/s41467-018-06036-0)
34. Miyake F, Hakozaki M, Kimura K, Tokanai F, Nakamura T, Takeyama M, Moriya T. 2022 Regional differences in carbon-14 data of the 993 CE cosmic ray event. *Front. Astron. Space Sci.* **9**, 886140. (doi:10.3389/fspas.2022.886140)
35. Nakamura T, Masuda K, Miyake F, Hakozaki M, Kimura K, Nishimoto H, Hitoki E. 2016 High-precision age determination of holocene samples by radiocarbon dating with accelerator mass spectrometry at Nagoya University. *Quat. Int.* **397**, 250–257. (doi:10.1016/j.quaint.2015.04.014)
36. Zhang Q, Sharma U, Dennis JA, Scifo A, Kuitems M, Büntgen U, Owens MJ, Dee MW, Pope BJS. 2022 Modelling cosmic radiation events in the tree-ring radiocarbon record. *Proc. R. Soc. A* **478**, 20220497. (doi:10.1098/rspa.2022.0497)
37. Golubenko K, Usoskin I, Rozanov E, Bard E. 2025 New SOCOL:14C-Ex model reveals that the late-glacial radiocarbon spike in 12350 BC was caused by the record-strong extreme solar storm. *Earth Planet. Sci. Lett.* **661**, 119383. (doi:10.1016/j.epsl.2025.119383)
38. Reimer PJ *et al.* 2020 The IntCal20 Northern Hemisphere radiocarbon calibration curve (0–55 kcal BP). *Radiocarbon* **62**, 725–757. (doi:10.1017/RDC.2020.41)
39. Usoskin IG, Solanki SK, Kovaltsov GA. 2007 Grand minima and maxima of solar activity: new observational constraints. *A&A* **471**, 301–309. (doi:10.1051/0004-6361:20077704)
40. Rato RT, Ortigueira MD, Batista AG. 2008 On the HHT, its problems, and some solutions. *Mech. Syst. Sig. Process.* **22**, 1374–1394. (doi:10.1016/J.YMSSP.2007.11.028)
41. Mekhaldi F, Adolphi F, Herbst K, Muscheler R. 2021 The signal of solar storms embedded in cosmogenic radionuclides: detectability and uncertainties. *J. Geophys. Res. Space Phys.* **126**, e2021JA029351. (doi:10.1029/2021JA029351)
42. Zhao W *et al.* 2026 Supplementary material from: Reassessment of a cosmic ray increase event in 1279/1280 CE using carbon-14 records of tree rings. Figshare. (doi:10.6084/m9.figshare.c.8571483)